Chemical tools to modulate endocannabinoid biosynthesis
Deng, H.

Cover Page

The handle http://hdl.handle.net/1887/47846 holds various files of this Leiden University dissertation

Author: Deng, Hui
Title: Chemical tools to modulate endocannabinoid biosynthesis
Issue Date: 2017-04-11

[^{18}F]DH439, a positron emission tomography tracer for *in vivo* imaging of diacylglycerol lipases*

Introduction

The endocannabinoid system is a lipid signaling network that regulates several (patho)physiological processes, including anxiety, depression, pain, inflammation, hepatic steatosis, neurodegeneration and obesity.[1,2] 2-Arachidonoylglycerol (2-AG) and anandamide (AEA) are the most abundant endocannabinoids, and activate type-1 and type-2 G protein-coupled cannabinoid receptors (CB$_1$R and CB$_2$R), thereby modulating neurotransmission and immune responses.[3] Early efforts focused on direct pharmacological intervention of the endocannabinoid system by various CB receptor agonists and antagonists, such as the classical CB$_1$R/CB$_2$R agonist Δ^9-tetrahydrocannabinol (THC) and the synthetic CB$_1$R antagonist Rimonabant.[1,2,4,5] However, concomitant adverse effects have limited their use as therapeutic agents. To solve this problem, an indirect approach by targeting the enzymes that regulate endogenous endocannabinoid levels has emerged as an alternative drug discovery strategy.[6]

Several inhibitors of monoacylglycerol lipase (MAGL) and fatty acid amide hydrolase (FAAH), which are the principal enzymes that degrade 2-AG and AEA, respectively,[7-9] are currently under clinical investigation as an alternative for THC.[6,8,10] By contrast, no inhibitors are available to reduce endocannabinoid formation in humans. Recently, compound **1** (DH376) was discovered as a brain active diacylglycerol lipase inhibitor (see Chapters 2-4). DH376 contains a 1,2,3-triazole urea and irreversibly inhibits DAGLs via carbamoylation of the active-site serine nucleophile. Pharmacological blockade of DAGLs by DH376 reduced 2-AG content in mouse brain as well as arachidonic acid (AA) and pro-inflammatory prostaglandins levels (Chapter 3). DH376 also reduced proinflammatory cytokines levels, prevented neuroinflammation in lipopolysaccharide-treated mice (Chapter 3) and reduced food intake in fasted mice (Chapter 4). This makes DH376 an interesting starting point for novel therapies aimed at treating the metabolic syndrome and/or neuroinflammatory disorders.

An important step in the translation of preclinical results from drug discovery towards the clinic is the demonstration of target engagement in animals and humans. Molecular imaging is the most frequently used technique to visualize inhibitor-target interactions in humans.[10-12] For example, positron emission tomography (PET) is a nuclear imaging technique that can be used to observe metabolic processes in the body.[13] Currently, no PET radiotracers for DAGL have been reported in the literature. A selective DAGL radiotracer will enable a more detailed assessment of DAGL distribution and DAGL activity in various tissues and will provide a tool for target engagement studies to guide dose selection in clinical trials. In this Chapter the first selective PET tracer for DAGL is described based on the structure of DH376.
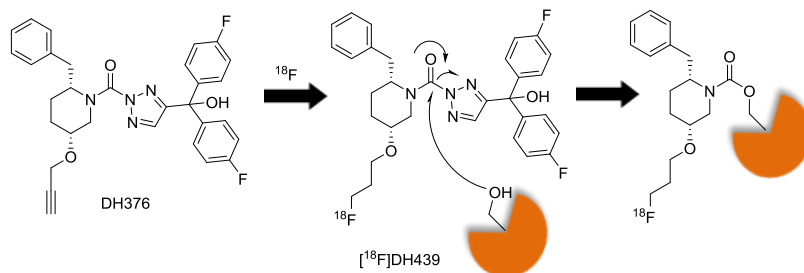

Figure 1. Design of PET radiotracer [18F]DH439(2) for DAGL using the mechanism-based and irreversible *in vivo* active DAGL inhibitor DH376.

Results and Discussion

Design and profiling of DH439, a fluorinated analog of DH376

[^{18}F]DH439 was designed as a covalent DAGL PET tracer that retains the activity and selectivity profile of DH376, but will also allow the radioactive labeling of the enzyme (Figure 1). The propargyl ether of DH376 was replaced with a 3-fluoropropylether in DH439. The chemical synthesis of compound **3** (DH439) started with the chiral intermediate *tert*-butyl-(*2R,5R*)-2-benzyl-5-hydroxypiperidine-1-carboxylate **6**, which was synthesized using previously reported methods (Scheme 1).[14,15] Treatment of alcohol **6** with sodium hydride in the presence of 3-fluoropropyl 4-methylbenzenesulfonate **5**, obtained from the commercially available 3-fluoropropan-1-ol **4**, afforded ether **7**. Removal of the Boc-protecting group using 20% TFA in DCM (v/v) and subsequent triphosgene-mediated coupling with 1,2,3-triazole **9** (synthesized as described in Chapter 2) in the present of catalytic amount of DMAP provided the final compound **3** in 30% yield over the three steps.
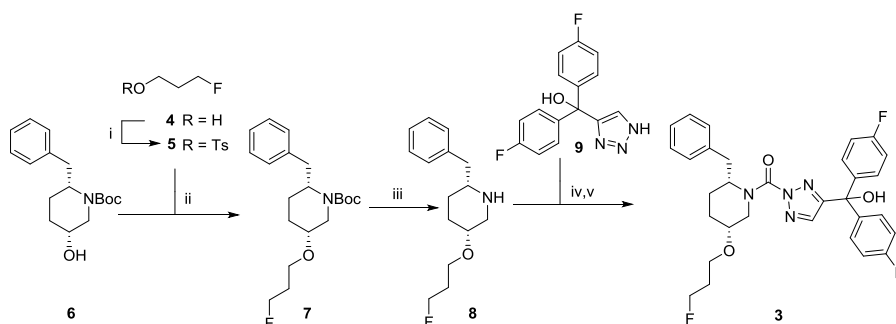
Scheme 1. Synthesis of compound **3** (DH439). Reagents and conditions: i) pTsCl, pyridine, DCM, r.t, 86%; ii) NaH, compound **5**, DMF, r.t., 19%; iii) 20% TFA, DCM, r.t.; iv) DIPEA, triphosgene, THF, 0 ^{o}C; v) DIPEA, DMAP, triazole **9**, THF, 60 ^{o}C, 30%.

Competitive activity-based protein profiling (ABPP) was employed to determine the activity and selectivity of fluorine-containing DH439 on endogenously expressed DAGL in mouse brain membrane proteome.[14] Briefly, DH439 was incubated for 20 min with mouse brain membrane homogenates, followed by two different activity-based probes (ABPs): DAGL-tailored ABP DH379 (described in Chapter 3) and broad-spectrum serine hydrolase ABP FP-TAMRA. DH379 provided target engagement assays for DAGLα and -β, and FP-TAMRA assessed selectivity over a broad array of brain serine hydrolases. DH439 potently inhibited DAGLα and DAGLβ labeling by DH379 with pIC$_{50}$ values of 9.3±0.1 and 9.2±0.1, respectively (Figure 2). Furthermore, DH439 maintained good selectivity over other serine hydrolases with

minimal cross-reactivity against ABHD6 at high concentration ($\geq$ 1 µM) (Figure 2a,b). In addition, DH439 showed negligible binding to cannabinoid CB_1 receptor, however, 64±14% displacement of [^{3}H]-CP55940 on the CB_2 receptor at concentrations $\geq$ 1 µM was observed (Figure 3).[16]
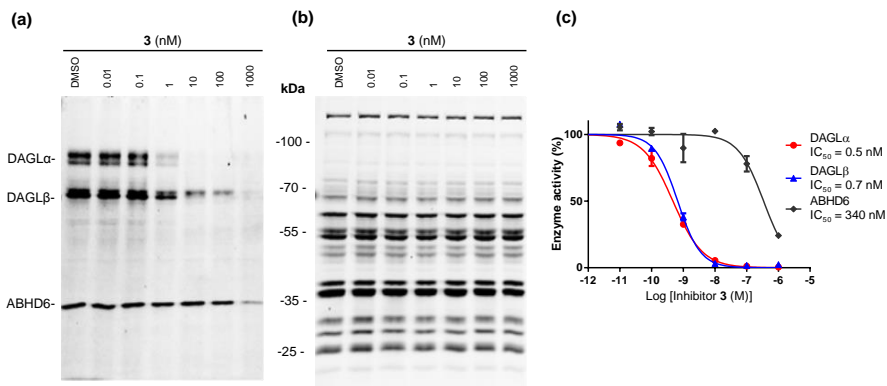

Figure 2. *In vitro* activity and selectivity profile of fluorine-containing DAGL inhibitor **3** (DH439) as measured by competitive ABPP. (a, b) Gel-based competitive ABPP of **3** using DH379 (a) and FP-TAMRA (b) as ABPs in mouse brain membrane proteome. (c) Concentration-inhibition curves for DAGLα, DAGLβ and ABHD6 as measured by competitive ABPP with ABP DH379 (1 µM). Data represent average ±SEM, n=3.
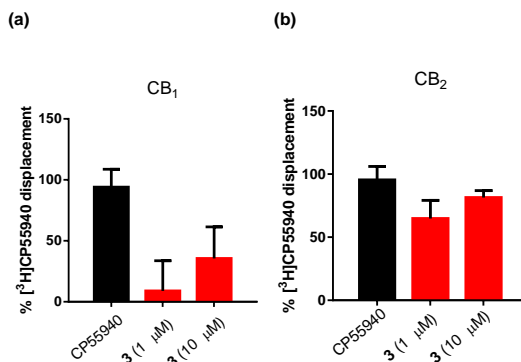
Figure 3. DAGL inhibitor **3** (DH439) shows variable interactions with CB_1 and CB_2. DH439 was tested for binding affinity to the CB_1 and CB_2 receptors using competition studies with radiolabeled CBR ligand [^{3}H]-CP55940 using membranes from recombinant human CB_1- and CB_2-overexpressing CHO cells. For CB_1, **3** was inactive at 1 µM and partial inhibition (35±25%) of ligand binding at 10 µM. For CB_2, **3** showed 64±14% and 81±5% inhibition of ligand binding at 1 µM and 10 µM, respectively. Data represent average ±SD, n=2.
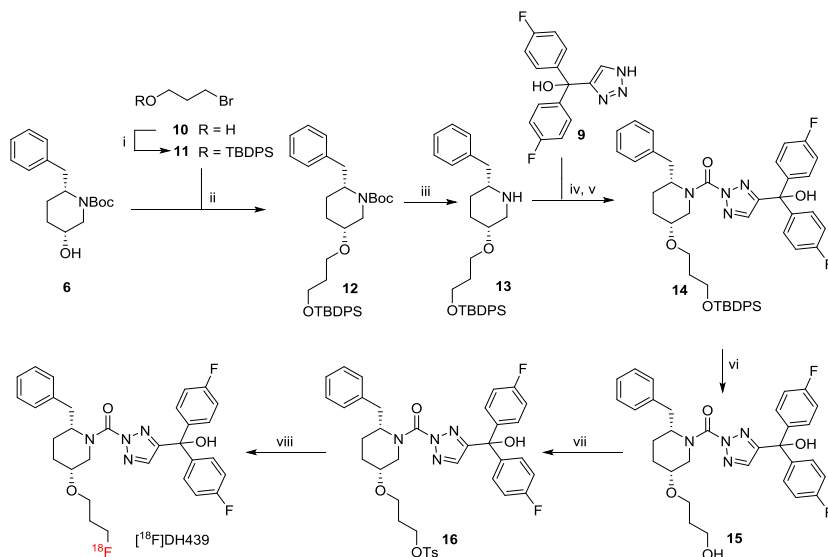
Scheme 2. Synthesis of PET radiotracer [^{18}F]DH439. Reagents and conditions: i) Imidazole, DMAP, TBDPS-Cl, DCM, r.t., 87%; ii) NaH, compound **11**, DMF, 87%; iii) 20% TFA, DCM, r.t.; iv) DIPEA, triphosgene, THF, 0 ^{o}C; v) DIPEA, DMAP, triazole **9**, THF, 60 ^{o}C; vi) HF-pyridine, THF : pyridine (1:1), 22% over 4 steps; vii) pTsCl, pyridine, DCM, r.t, 63%; viii) Micro reactor chip, K$_2$CO$_3$, TBA [^{18}F], CH$_3$CN, 95 min, 13-14%.

Synthesis of the fluorine-containing DAGL inhibitor and PET tracer, [^{18}F]DH439

Having established that DH439 retains a favorable activity and selectivity profile, compound **16** was prepared as an essential building block for the synthesis of [^{18}F]DH439 (Scheme 2), since it contains a tosylate required for the fluorination in the final step of the synthesis of **2** ([^{18}F]DH439). The synthesis of **16** commenced with the treatment of **6** with **11** prepared from commercially available 3-bromopropan-1-ol **10**, providing *O*-silyl protected intermediate **12**. *N*-Boc deprotection of **12** and subsequent coupling of the resulting product **13** to 1,2,3-triazole **9** furnished intermediate **14**, which was deprotected with HF-pyridine to provide alcohol **15** in 22% yield over four steps. Tosylation of **15** afforded the desired radiolabeling precursor **16** in 67% yield.

To substitute the tosylate of precursor **16** with the radiolabel (^{18}F), flow chemistry was employed by using a microreactor chip (FlowSafe - Future Chemistry). In brief, precursor **16** and [^{18}F]fluoride were transferred to a 110 µL microfluidic reactor chip and reacted in acetonitrile for 95 min. After a reversed-phase preparative HPLC purification, [^{18}F]DH439 was obtained in a radiochemical yield of 13-14% (decay corrected). The amount of activity obtained for the studies was 40-54 MBq. The

radiochemical purity of [^{18}F]DH439 as determined by analytical radio-HPLC was >98% (Figure 4).
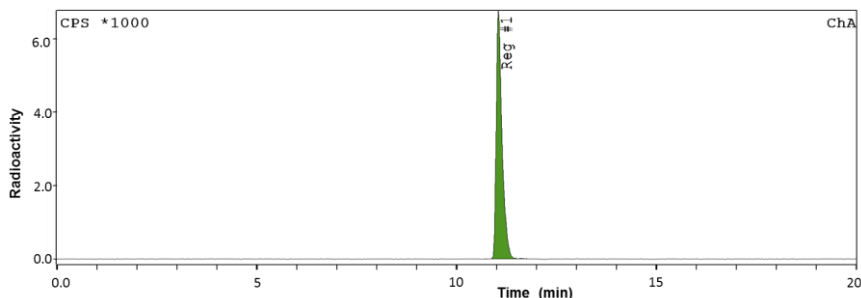

Figure 4. The radiochemical purity of [^{18}F]DH439 (**2**) was determined by analytical radio-HPLC (>98%).

In vivo biodistribution and PET imaging in a pilot mice study

Initial *in vivo* evaluation of [^{18}F]DH439 was conducted in male C57BL/6 (n = 3 per group) with intravenous injection. A bolus of 4-10 MBq [^{18}F]DH439 and DH439 (0.8 mg/kg) was injected intravenously using in saline/ethanol/tween-80 (18:1:1; v/v/v) as a vehicle. The additional injection of DH439 (0.8 mg/kg) was performed to reduce non-specific binding and metabolism of [^{18}F]DH439. Results of the biodistribution study in mice are presented in Figure 5. [^{18}F]DH439 displayed good uptake in several peripheral tissues after 140 min injection, and particularly in liver and kidney (Figure 5). Previously, DAGLα was found to be highly active in the brain (see Chapter 4), whereas DAGLβ activity was also found in heart, lung, kidney, pancreas, spleen and testis. In the PET-study only a trace amount of tracer uptake was observed in the brain. It could be that [^{18}F]DH439 has low blood-brain barrier (BBB) penetration, or, alternatively, [^{18}F]DH439 is not stable and quickly metabolized. The high amount of radioactivity in liver (Figure 5) might be an indication for the extensive metabolism of [^{18}F]DH439. Thus, it would be interesting to determine the rate of tracer metabolism by radio-metabolite analysis on blood samples and organs of interest with radio-HPLC. In addition, an important characteristic of a good PET tracer is the stability of the bond between the radionuclide and the molecule of interest. When the ^{18}F-C bond is unstable, the fluorine-18 atom could be cleaved and will accumulate in the bone. A slow accumulation of radioactivity was observed in the bone (Femur) (Figure 5), indicating some de-fluorination occurred. However, there was still sufficient amount of radioactivity in other organs, therefore de-fluorination does not seem to limit the application of the PET tracer [^{18}F]DH439 in mice.
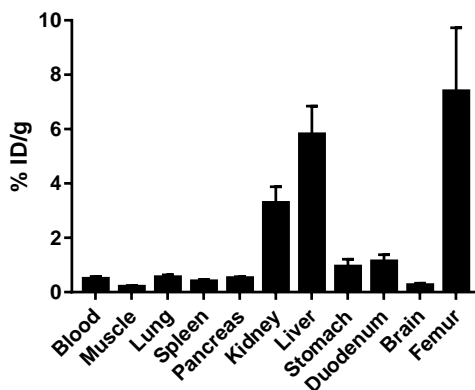
Figure 5. Bio-distribution (% ID/g) in mice (n=3; mean ± SEM) at 140 min after injection of radio tracer [^{18}F]DH439.

Next, an *in vivo* PET imaging was performed (Figure 6). This study generated comparable results to the biodistribution experiment. PET imaging showed the highest accumulation in liver and kidney. The representative dynamic PET images of [^{18}F]DH439 and time-activity curves at baseline with treatment of [^{18}F]DH439 are shown in Figure 6. [^{18}F]DH439 exhibited highly sustained binding in bladder, liver and kidney over 120 mins. PET-imaging showed that [^{18}F]DH439 accumulated slowly in the brain, which is in line with the biodistribution study. A dramatic increase in radioactivity in the kidney was also observed (Figure 6b). However, to confirm target engagement and to exclude non-specific binding of [^{18}F]DH439 further experiments are needed. For example, these experiments could include raising the dose of [^{18}F]DH439 to increase brain penetration; pretreat the mice with unlabeled DH439 to induce self-blockade, inject a specific ABHD6 inhibitor to exclude ABHD6 binding, or administer another selective DAGL inhibitor to confirm DAGL binding. Considering the low tracer uptake in the brain, further radiotracer optimization may also be required to improve brain penetration and *in vivo* stability.

(a)

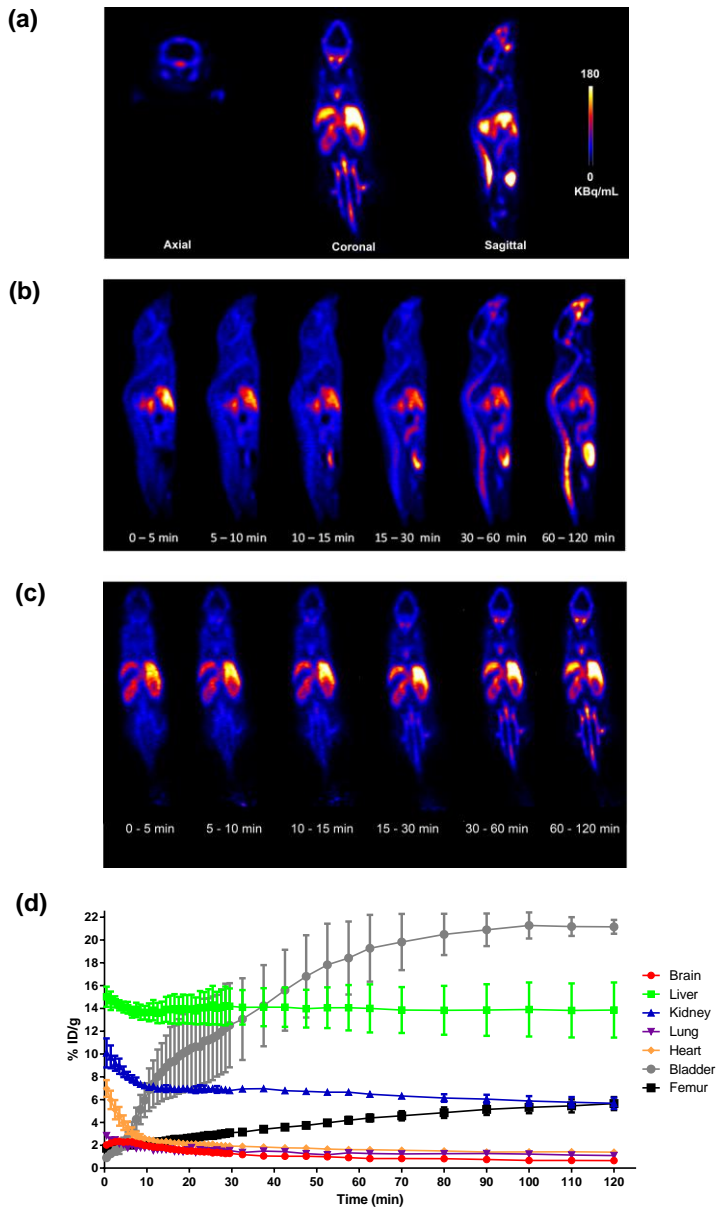

(b)

(c)

(d)

Figure 6. (a) Representative 2D reconstructed PET Images (0-120 min; axial, coronal and sagittal sections). (b-c) Representative 2D reconstructed dynamic PET images of [^{18}F]DH439-treated mice at various time frames (b for sagittal sections and c for coronal sections). (d) Time-activity curves from [^{18}F]DH439 at baseline in mice (n=3; mean ± SEM).

Conclusion

In summary, the first selective DAGL PET tracer [^{18}F]DH439 was designed and synthesized. As assessed by competitive ABPP and radioligand displacement assays, DH439 showed high potency and selectivity against DAGLs, but some minor affinity towards the cannabinoid CB$_2$ receptor was also identified. Biodistribution experiments of [^{18}F]DH439 in mice revealed low tracer uptake in the brain and high uptake in peripheral tissues such as liver and kidney. *In vivo* mouse PET imaging studies mirrored those of the biodistribution studies. Although this work was a pilot study, it demonstrated the feasibility of generating PET tracers from 1,2,3-triazole urea inhibitors for preclinical studies. These studies may pave the way for the development of clinical PET tracers of DAGL to study biodistribution and target engagement of DAGLs in humans and to guide dose selection for human clinical trials. An improvement in metabolic stability and brain penetration is required to obtain a suitable PET tracer to study target engagement of DAGL inhibitors in the brain.

Experimental section

Chemistry

General materials

All chemicals were obtained from commercial suppliers and were used without further purification. TLC analysis with Merck silica gel TLC plates (0.25 mm, 60/Kieselguhr F254) was used to monitor reactions. Flash chromatography was performed using SiliaFlash F60 silica gel (40–63 µm, 60 Å). NMR spectra were recorded at room temperature on Bruker AV 400 MHz spectrometer at 400 (^{1}H) and 101 (^{13}C) MHz using CDCl$_3$ as solvent. Chemical shifts are recorded in ppm relative to tetramethylsilane (TMS) with peaks being reported as follows: chemical shift, multiplicity (s = singlet, br = broad, d = doublet, t = triplet, q = quartet, m = multiplet), coupling constant (Hz). High-resolution mass spectra (HRMS) were recorded by direct injection (2 µL of a 2 µM solution in water/acetonitrile 50/50 (v/v) and 0.1% formic acid) on a mass spectrometer (Thermo Finnigan LTQ orbitrap) equipped with an electrospray ion source in positive mode (source voltage 3.5 kV, sheath gas flow 10, capillary temperature 250 ^{o}C) with resolution R = 60,000 at m/z 400 (mass range m/z = 150-2,000) and dioctylphthalate (m/z = 391.28428) as a "lock mass". The high resolution mass spectrometer was calibrated prior to measurements with a calibration mixture (Thermo Finnigan). LC-MS analysis was performed on a Finnigan Surveyor HPLC system with a Gemmi C$_{18}$ 50x4.60 mm column (detection at 200-600 nm), coupled to a Finnigan LCQ Adantage Max mass spectrometer with ESI. The applied buffers were H$_2$O, MeCN and 1.0% TFA in H$_2$O (0.1% TFA end concentration). Optical

rotations were measured on a Propol automatic polarimeter (Sodium D-line, λ = 589 nm).

Radiolabeling

Radiochemistry was performed using a flow reaction on a reactor chip in Future Chemistry's FlowSafe. [^{18}F]fluoride in acetonitrile was purchased from commercial sources. A reversed phase preparation HPLC method was setup to isolate [^{18}F]DH439 and a SPE procedure was applied to remove the acetonitrile from the pooled HPLC peak and to reformulate [^{18}F]DH439 in 80:10:10 NaCl (0.9%)/ethanol/Tween-80 (v/v/v). The identity of the labeled compound was confirmed by co-injection of the authentic on HPLC. The specific activity was determined by injection of an aliquot of the final solution with known radioactivity on the analytical HPLC system described above. The area of the UV peak measured at 254 nm corresponding to the carrier product was measured and compared to a standard curve relating mass to UV absorbance. Radioactivity was measured with a Capintec CRC-15 PET dose calibrator.

Synthesis

((*2R,5R*)-2-Benzyl-5-(3-fluoropropoxy)piperidin-1-yl)(4-(bis(4-fluorophenyl)(hydroxy)methyl)-*2H*-1,2,3-triazol-2-yl)methanone (3). A solution of compound **8** in THF was treated with DIPEA (0.38 mL, 2.19 mmol) and bis(trichloromethyl) carbonate (65.0 mg, 0.22 mmol). The reaction mixture was stirred for 30 min at 0 °C, then the mixture was poured into water and extracted with EtOAc (3 x 50 mL).The organic layer was washed with water, brine, dried over MgSO$_4$, filtered and concentrated under reduced pressure. The intermediate was dissolved in THF and DIPEA (0.38 mL, 2.19 mmol), DMAP (54 mg, 0.44 mmol) and compound **9** (126 mg, 0.438 mmol) were added to the solution. The mixture was stirred for 2 h at 60 °C and poured into saturated aqueous NH$_4$Cl solution. The mixture was extracted with EtOAc, washed with water, brine, dried over MgSO$_4$, filtered and concentrated under reduced pressure. The residue was purified by silica gel column chromatography with acetone/pentane (1%→10%) to yield the target compound DH439 (**3**) (74 mg, 0.13 mmol, 30% yield). HRMS calculated for [C$_{31}$H$_{32}$F$_3$N$_4$O$_3$]$^+$: 565.24210; found: 565.24218; ^{1}H NMR (400 MHz, CDCl$_3$) δ 7.52 (br, 1H), 7.34 – 7.24 (m, 6H), 7.18 (br, 2H), 7.05 – 7.00 (m, 4H), 6.89 (br, 1H), 4.79 – 4.24 (m, 4H), 3.71 (br, 1H), 3.53 – 3.43 (m, 2H), 3.16 – 2.85 (m, 3H), 2.10 – 1.84 (m, 3H), 1.77 – 1.62 (m, 3H); ^{13}C NMR (101 MHz, CDCl$_3$) δ 162.48 (d, *J* = 252.9 Hz), 157.74, 149.03, 140.71 (d, *J* = 3.0 Hz), 137.64, 135.32, 129.17 (d, *J* = 7.1 Hz), 129.05, 128.84, 126.95, 115.34 (d, *J* = 22.2 Hz), 81.02 (d, *J* = 170.7 Hz), 77.16, 76.60, 74.28, 64.36, 56.61, 44.47, 35.62, 31.14 (d, *J* = 20.2 Hz), 26.03, 25.97.

3-Fluoropropyl 4-methylbenzenesulfonate (5). To a solution of pyridine (0.725 mL, 8.96 mmol) in dry DCM was added 3-fluoropropan-1-ol (0.337 mL, 4.48 mmol) and *p*-toluenesulfonyl chloride (1.03 g, 5.38 mmol) at 0 °C. The reaction mixture was stirred for 24 h at r.t. The mixture was diluted with water and extracted with DCM. The organic layer was washed with brine, dried over MgSO$_4$, filtered and evaporated under

reduced pressure. The residue was purified by silica gel column chromatography with diethyl ether/pentane (1%→10%) to yield 3-fluoropropyl 4- methylbenzenesulfonate **5** (895 mg, 3.85 mmol, 86% yield). LC/MS calculated for $[C_{10}H_{13}FO_3S]^+$: 232.27; found: 233.02; ^{1}H NMR (400 MHz, CDCl$_3$) δ 7.79 (d, J = 8.3 Hz, 2H), 7.36 (d, J = 8.2 Hz, 2H), 4.54 (t, J = 5.7 Hz, 1H), 4.42 (t, J = 5.7 Hz, 1H), 4.15 (t, J = 6.2 Hz, 2H), 2.45 (s, 3H), 2.07 (p, J = 5.9 Hz, 1H), 2.00 (p, J = 5.9 Hz, 1H). ^{13}C NMR (101 MHz, CDCl$_3$) δ 145.06, 132.73, 129.98, 128.00, 79.58 (d, J = 166.7 Hz), 66.28, 30.00 (d, J = 20.2 Hz) 21.67.

tert-Butyl (_2R,5R_)-2-benzyl-5-(3-fluoropropoxy)piperidine-1-carboxylate (7). To a solution of compound 6 (228 mg, 0.783 mmol) and NaH (78 mg, 1.96 mmol) in DMF (10 mL) at 0 °C, 3-fluoropropyl 4-methylbenzenesulfonate (200 mg, 0.86 mmol) was added dropwise with continuous stirring, and the mixture was allowed to stand at r.t. for 24 h. The mixture was diluted with water (50 mL), and extracted with EtOAc (80 mL x 3). The organic layers were washed with water, brine, dried over MgSO$_4$, filtered and concentrated under reduced pressure. The residue was then purified by silica gel column chromatography with diethyl ether/pentane (1%→20%) to yield _tert_-butyl (_2R,5R_)-2-benzyl-5-(3-fluoropropoxy)piperidine-1-carboxylate (53.0 mg, 0.151 mmol, 19% yield). LC/MS calculated for $[C_{20}H_{30}FNO_3]^+$: 351.46; found: 351.98; ^{1}H NMR (400 MHz, CDCl$_3$) δ 7.30 – 7.24 (m, 2H), 7.24 – 7.12 (m, 3H), 4.61 (t, J = 5.9 Hz, 1H), 4.49 (t, J = 5.9 Hz, 1H), 4.44 – 4.29 (m, 1H), 3.68 – 3.60 (m, 2H), 3.26 (br, 1H), 2.96 – 2.85 (m, 1H), 2.76 – 2.63 (m, 2H), 2.02 – 1.89 (m, 3H), 1.59 (d, J = 9.2 Hz, 3H), 1.27 (s, 9H); ^{13}C NMR (101 MHz, CDCl$_3$) δ 154.87, 139.14, 129.27, 128.52, 126.34, 81.15 (d, J = 164.6 Hz), 79.69, 74.83, 64.28, 52.21, 42.47, 35.97, 31.24 (d, J = 20.2 Hz), 28.28, 26.32, 26.10.

(_2R,5R_)-2-Benzyl-5-(3-fluoropropoxy)piperidine (8). To a solution of _tert_-butyl (_2R,5R_)-2- benzyl-5-(3-fluoropropoxy)piperidine-1-carboxylate **7** (351 mg, 0.597 mmol) in DCM was added TFA (20%, v/v), the reaction mixture was stirred at r.t. for 2.5 h until TLC showed the reaction was completed. The mixture was co-evaporated with toluene (3 x 20 mL), the residue was diluted with EtOAc and washed with 10% Na$_2$CO$_3$, water, brine, dried over MgSO$_4$, filtered and then concentrated under reduced pressure. The crude product was used for next step without further purification. ^{1}H NMR (400 MHz, CDCl$_3$) δ 7.31 – 7.22 (m, 3H), 7.17 (d, J = 7.0 Hz, 2H), 4.58 (t, J = 4.7 Hz, 1H), 4.47 (t, J = 4.6 Hz, 1H), 3.69 (s, 1H), 3.55 (q, J = 6.0 Hz, 2H), 3.45 (d, J = 12.2 Hz, 1H), 3.28 (s, 1H), 3.14 (d, J = 13.2 Hz, 1H), 3.05 (s, 1H), 2.89 – 2.79 (m, 1H), 2.06 (d, J = 12.8 Hz, 1H), 2.00 – 1.93 (m, 1H), 1.93 – 1.88 (m, 1H), 1.83 (d, J = 13.5 Hz, 1H), 1.64 (d, J = 13.1 Hz, 1H), 1.50 (d, J = 13.1 Hz, 1H). ^{13}C NMR (101 MHz, CDCl$_3$) δ 135.11, 129.48, 128.98, 127.46, 80.97 (d, J = 163.6 Hz), 69.04, 64.39, 58.19, 47.59, 39.60, 30.62 (d, J = 20.2 Hz), 26.07, 22.79.

(3-Bromopropoxy)(_tert_-butyl)diphenylsilane (11). _tert_-Butyl(chloro)diphenylsilane (4.62 mL, 18.0 mmol), DMAP (0.611 g, 5.0 mmol) and imidazole (1.40 g, 20.0 mmol) were added to a stirred solution of 3-bromopropan-1-ol (0.91 mL, 10.0 mmol) in DCM with ice cooling, and then stirred at r.t. for 2 h. The resulting mixture was quenched

with water, and extracted with EtOAc (3 x 80 mL). The combined organic layers were washed with water, brine, dried over $MgSO_4$, filtered and concentrated under reduced pressure. The residue was purified by silica gel column chromatography with diethyl ether/pentane (1%→10%) to yield compound **11** (3.28 g, 8.70 mmol, 87% yield). LC/MS calculated for $[C_{19}H_{25}BrOSi]^+$: 377.40; found: 378.12; ^{1}H NMR (400 MHz, CDCl₃) δ 7.76 – 7.57 (m, 4H), 7.52 – 7.25 (m, 6H), 3.77 (t, *J* = 5.7 Hz, 2H), 3.57 (t, *J* = 6.6 Hz, 2H), 2.08 – 2.03 (m, 2H), 1.06 (s, 9H). ^{13}C NMR (101 MHz, CDCl₃) δ 135.20, 134.95, 129.67, 127.76, 26.67, 19.06.

tert-Butyl (_2R,5R_)-2-benzyl-5-(3-((_tert_-butyldiphenylsilyl)oxy)propoxy)piperidine-1-carboxylate (12). To a solution of compound **6** (200 mg, 0.69 mmol) and NaH (82.0 mg, 2.06 mmol) in DMF (4 mL) at 0 °C, compound **11** (777 mg, 2.06 mmol) was added dropwise under continuous stirring, and the mixture was allowed to stand at r.t. for 24 h. The mixture was diluted with water (20 mL), the residue of a product filtered off, washed with water, brine, dried over $MgSO_4$, filtered and concentrated under reduced pressure. The residue was purified by silica gel column chromatography with diethyl ether/pentane (1%→10%) to yield compound **12** (351 mg, 0.60 mmol, 87% yield). LC/MS calculated for $[C_{36}H_{49}NO_4Si]^+$: 587.88; found: 588.20; ^{1}H NMR (400 MHz, CDCl₃) δ 7.80 – 7.73 (m, 5H), 7.49 – 7.38 (m, 6H), 7.34 – 7.30 (m, 2H), 7.24 – 7.20 (m, 2H), 4.54 – 4.21 (m, 2H), 3.83 (t, *J* = 5.8 Hz, 2H), 3.79 – 3.64 (m, 2H), 3.29 (br, 1H), 3.05 – 2.91 (m, 1H), 2.73 – 2.69 (m, 2H), 2.02 – 1.76 (m, 3H), 1.62 (d, *J* = 10.0 Hz, 3H), 1.44 (s, 3H), 1.34 (s, 6H), 1.12 (s, 9H). ^{13}C NMR (101 MHz, CDCl₃) δ 154.79, 139.17, 135.62, 134.91, 133.97, 133.93, 129.64, 129.57, 129.25, 128.49, 127.71, 127.70, 126.29, 79.59, 74.54, 65.38, 60.69, 52.28, 42.53, 36.00, 33.18, 26.95, 26.67, 26.34, 26.12, 19.31.

((_2R,5R_)-2-Benzyl-5-(3-hydroxypropoxy)piperidin-1-yl)(4-(bis(4-fluorophenyl)(hydroxy)methyl)-2_H_-1,2,3-triazol-2-yl)methanone (15). To a solution of compound **12** (351 mg, 0.597 mmol) in DCM was added TFA (20%, v/v), the reaction mixture was stirred at room temperature for 2.5 h until TLC analysis showed that the reaction was completed. The mixture was co-evaporated with toluene (3 x 20 mL), the residue was diluted with EtOAc and washed with 10% Na_2CO_3, water, brine, dried over $MgSO_4$, filtered and then concentrated under reduced pressure. The crude product was used for next step without further purification. A solution of the crude product **13** in THF was treated with DIPEA (0.524 mL, 3.0 mmol) and bis(trichloromethyl) carbonate (89.0 mg, 0.30 mmol) and the reaction mixture was stirred for 30 min at 0 °C. The mixture was poured into water and extracted with EtOAc (40 mL x 3). The organic layer was washed with water, brine dried over $MgSO_4$, filtered and concentrated under reduced pressure. The intermediate was dissolved in THF and DIPEA (0.31 mL, 1.80 mmol), DMAP (74.0 mg, 0.60 mmol) and triazole **9** (172 mg, 0.60 mmol) were added to the solution. The mixture was stirred for 2 h at 60°C and poured into saturated aqueous NH_4Cl solution and extracted with EtOAc, washed with water, brine, dried over $MgSO_4$, and concentrated under reduced pressure. The N2-carbamoyl triazole urea **14** was isolated by silica gel chromatography EtOAc/pentane (1%→10%). HF-pyridine (0.60 mL, 6.50 mmol) was subsequently added to a solution of N2-carbamoyl triazole urea in THF and pyridine (1:1; 2 mL) with ice cooling, and the reaction mixture was

stirred over night at r.t. The mixture was diluted with EtOAc (40 mL), and then washed with NaHCO$_3$, brine, dried with MgSO$_4$, and concentrated under reduced pressure. The residue was purified by silica gel column chromatography with EtOAc /pentane (1%→40%) to yield the title compound **15** (73 mg, 0.13 mmol, 22% yield) as a colorless oil. LC/MS calculated for [C$_{31}$H$_{32}$F$_2$N$_4$O$_4$]$^+$: 562.62; found: 567.13; ¹H NMR (400 MHz, CDCl$_3$) δ 7.52 (s, 1H), 7.41 – 7.15 (m, 8H), 7.07 – 6.84 (m, 5H), 4.54 (br, 1H), 4.31 (br, 1H), 3.80 – 3.58 (m, 4H), 3.50 – 3.44 (m, 1H), 3.17 – 2.86 (m, 3H), 2.04 (d, *J* = 7.9 Hz, 1H), 1.85 – 1.59 (m, 5H). ¹³C NMR (101 MHz, CDCl$_3$) δ 162.36 (d, *J* = 252.5 Hz), 155.71, 149.27, 140.84 (d, *J* = 5.1 Hz), 137.57, 135.44, 129.13 (d, *J* = 9.1 Hz), 128.78, 126.89, 124.28, 115.20 (d, *J* = 22.4 Hz), 76.37, 74.41, 67.61, 61.39, 55.69, 46.06, 35.80, 32.22, 25.96, 25.06.

3-(((*3R,6R*)-6-Benzyl-1-(4-(bis(4-fluorophenyl)(hydroxy)methyl)-2*H*-1,2,3-triazole-2-carbonyl)piperidin-3-yl)oxy)propyl 4-methylbenzenesulfonate (16). To a solution of compound **15** (60.0 mg, 0.11 mmol) and pyridine (0.03 mL, 0.32 mmol) in dry DCM was added pTsCl (61.0 mg, 0.32 mmol) at 0 °C. The reaction mixture was stirred for 24 h at r.t. The mixture was quenched with water and extracted with DCM. The organic layer was washed with brine, dried over MgSO$_4$, filtered and co-evaporated under reduced pressure. The residue was purified by silica gel column chromatography EtOAc/pentane (1%→20%) to yield the title compound **16** (50 mg, 0.069 mmol, 63% yield). LC/MS calculated for [C$_{38}$H$_{38}$F$_2$N$_4$O$_6$S]$^+$: 716.80; found: 717.03; ¹H NMR (400 MHz, CDCl$_3$, 60 °C) δ 7.76 (d, *J* = 7.9 Hz, 2H), 7.54 (s, 1H), 7.36 – 7.26 (m, 6H), 7.26 – 7.16 (m, 4H), 6.98 (t, *J* = 8.3 Hz, 5H), 4.48 (s, 1H), 4.13 (t, *J* = 4.0 Hz, 2H), 3.49 (br, 2H), 3.40 – 3.35 (m, 2H), 3.05 (dd, *J* = 13.4, 6.4 Hz, 1H), 2.90 (t, *J* = 12.0 Hz, 2H), 2.42 (s, 3H), 1.89 (d, *J* = 26.6 Hz, 3H), 1.65 (br, 3H); ¹³C NMR (101 MHz, CDCl$_3$, 60 °C) δ 162.55 (d, *J* = 248.5 Hz), 155.74, 149.41, 144.87, 140.98 (d, *J* = 5.1 Hz), 137.76, 135.26, 133.72, 129.98, 129.20 (d, *J* = 8.1 Hz), 128.83, 128.01, 126.93, 115.26 (d, *J* = 21.2 Hz), 76.69, 74.39, 67.45, 64.29, 55.18, 45.62, 36.11, 29.71, 26.07, 25.14, 21.66.

Biological assays

Fluorophosphonate-TAMRA (FP-TAMRA), and DH379 were synthesized according to a previously described protocol.[17-21] FP-TAMRA is also commercially available at Thermo Fischer Scientific.

Preparation of tissue proteomes

Mouse tissues were dounce homogenized in lysis buffer (20 mM HEPES, 250 mM sucrose, 2 mM DTT, 1 mM MgCl$_2$ with or without 25 U/mL benzonase) and incubated in ice for 5 min, followed by a low-speed spin (1,400−2,500 x g, 3 min, 4 °C) to remove debris. The membrane and cytosolic fractions were separated by ultracentrifugation (100,000 x g, 45 min, 4 °C) of the resulting homogenate lysate. After removal of the soluble supernatant, the membrane pellet was washed 1x with cold HEPES buffer (20 mM, with or without 2 mM DTT) followed by resuspension in cold HEPES buffer (20

mM, with or without 2 mM DTT) by pipetting. Total protein concentrations in membrane and soluble fractions were determined using the Bio-Rad DC protein assay kit. Samples were stored at -80 °C until further use.

Tissue profiling by gel-based competitive ABPP

Gel-based ABPP assays were performed as previously described (Chapter 3). Cell or tissue proteomes were treated with either FP-TAMRA (1 µM or 500 nM final concentration), DH379 (1 µM final concentration). For DH379 labeled samples, 2 mg/mL of proteome was used to enhance endogenous DAGL signals; 1 mg/mL proteome was used for labeling with FP-TAMRA. Probe labeling was carried out for 30 min at r.t. followed by addition of 4X SDS-PAGE loading buffer to quench the reaction. After separation by SDS-PAGE (10% acrylamide), samples were visualized by in-gel fluorescence scanning using a ChemiDoc MP system.

ABPP inhibitor activity measurements

The percentage of activity remaining was determined by measuring the integrated optical intensity of the fluorescent protein bands using image lab 4.1. The relative intensity was compared to the vehicle treated proteins, which were set to 100%. IC_{50} and IC_{80} values were determined by plotting a log(inhibitor) vs. normalized response (Variable slope) dose-response curve generated using Prism software (GraphPad).

Radioligand binding assay

Materials: [^{3}H]CP55940 (specific activity 141.2 Ci/mmol) and GF-C filters were purchased from Perkin Elmer (Waltham, MA). Bicinchoninic acid (BCA) and BCA protein assay reagent were obtained from Pierce Chemical Company (Rochford, IL). The PathHunter® CHO-K1 CNR1 β-Arrestin Cell Line (catalog number 93-0959C2) and the PathHunter® CHO-K1 CNR2 β-Arrestin Cell Line (catalog number 93-0706C2), stably expressing the hCB_1 receptor (CHOK1hCB$_1$_bgal) or hCB_2 receptor (CHOK1hCB$_2$_bgal) respectively, was obtained from DiscoveRx.

Cell culture and membrane preparation: CHOK1hCB$_1$_bgal and CHOK1hCB$_2$_bgal cells were cultured in Ham's F12 Nutrient Mixture supplemented with 10% fetal calf serum, 1 mM glutamine, 50 µg/mL penicillin, 50 µg/mL streptomycin, 300 mg/mL hygromycin and 800 µg/mL geneticin in a humidified atmosphere at 37 °C and 5% CO_2. Cells were subcultured twice a week at a ratio of 1:20 on 10-cm diameter plates by trypsinization. For membrane preparation the cells were subcultured 1:10 and transferred to large 15-cm diameter plates. Membrane fractions were prepared exactly as described before.[22]

[^{3}H]CP55940 radioligand binding assay: [^{3}H]CP55940 binding assays to determine the cannabinoid CB_1 and CB_2 receptor binding affinity were performed as follows: ligands of interest were incubated at 30°C for 1h with membrane aliquots containing 5 µg CHOK1hCB$_1$_bgal membrane protein or 1 µg (CHOK1hCB$_2$_bgal) in 100 µL assay

buffer (50 mM Tris–HCl, 5 mM $MgCl_2$, 0.1% BSA, pH 7.4) with [^{3}H]CP55940 in a concentration of ~1.5 nM (CB_2 receptor) or ~3.5 nM (CB_1 receptor) per assay point. Non-specific binding was determined in the presence of 10 μM Rimonabant (CB_1 receptor) or 10 μM AM630 (CB_2 receptor). Filtration was performed on GF/C filters, presoaked for 30 min with 0.25% polyethylenimine, using a Brandel harvester. Filter-bound radioactivity was determined in a β-counter. The mean % of specific binding for CB_1 and CB_2 receptors were 36 ± 4% and 38 ± 42% for 6-12 experiments.

PET imaging study and Biodistribution studies in mice

Mice (C75Bl/6J, male, 32.0±0.4 gram) were used for the animal experiments. A cannula was inserted into the lateral tail vein and anesthesia was induced using 2% isoflurane. The mice were placed prone in an Inveon animal PET/CT scanner (Siemens Preclinical Solutions). Anesthesia was maintained using 1.5% isoflurane via a nose cone and their body temperature was maintained at 35 °C using a heating bed. A bolus of 4-10 MBq [^{18}F]DH439 and 25.6 μg of DH439 in 200 μL saline/ethanol/Tween-80 (18:1:1; v/v/v) was injected intravenously via the cannula. The additional 25.6 μg of DH439 was added to adjust the dose to 0.8 mg/kg. A 125 minute dynamic emission PET scan was acquired. For attenuation correction followed by a 10 minute transmission scan using the built-in 57Co source. The mice were euthanized by CO_2/O_2 asphyxiation directly after the transmission scan. Mouse was subsequently placed in the CT scanner of the Inveon PET/CT (spatial resolution, 110 μm; 80 kV, 500 μA; spatial resolution of PET is 1.5 mm) to obtain a CT scan for anatomic reference. Of all mice, tissues of interest (blood, muscle, lung, spleen, pancreas, kidney, liver, stomach, duodenum, brain and femur) were dissected, weighed and counted in a γ-counter. The percentage injected dose per gram of tissue (%ID/g) was calculated for each tissue on the basis of a dilution of the product for injection ([^{18}F]DH439).

PET images were reconstructed using Inveon Acquisition Workplace software using 3D-OSEM in the following frames: 30 x 60s , 7 x 300s and 6 x 600s. The images were analyzed using Siemens Inveon Research Workplace software. Regions of interest (ROIs) were manually drawn over the organs of interest (brain, liver, kidney, lung, heart, bladder, and femur). Quantification of [^{18}F]DH439 uptake in the ROIs of the attenuation-corrected slices was obtained by calculating the injected dose per gram of wet tissue (%ID/g).

References

1. Pacher, P.; Kunos, G. Modulating the endocannabinoid system in human health and disease successes and failures. *FEBS Journal* **2013,** 280, 1918-1943.
2. Pertwee, R. G. The pharmacology of cannabinoid receptors and their ligands: an overview. *International Journal of Obesity* **2006,** 30, S13-S18.
3. Katona, I.; Freund, T. F. Multiple functions of endocannabinoid signaling in the brain. *Annual Review of Neuroscience, 35* **2012,** 35, 529-558.
4. Janero, D. R.; Makriyannis, A. Cannabinoid receptor antagonists: pharmacological opportunities, clinical experience, and translational prognosis. *Expert Opinion on Emerging Drugs* **2009,** 14, 43-65.
5. Kirilly, E.; Gonda, X.; Bagdy, G. CB1 receptor antagonists: new discoveries leading to new perspectives. *Acta Physiologica* **2012,** 205, 41-60.
6. Blankman, J. L.; Cravatt, B. F. Chemical Probes of Endocannabinoid Metabolism. *Pharmacological Reviews* **2013,** 65, 849-871.
7. McKinney, M. K.; Cravatt, B. F. Structure and function of fatty acid amide hydrolase. *Annual Review of Biochemistry* **2005,** 74, 411-432.
8. Ahn, K.; McKinney, M. K.; Cravatt, B. F. Enzymatic pathways that regulate endocannabinoid signaling in the nervous system. *Chemical Reviews* **2008,** 108, 1687-1707.
9. Long, J. Z.; Cravatt, B. F. The Metabolic Serine Hydrolases and Their Functions in Mammalian Physiology and Disease. *Chemical Reviews* **2011,** 111, 6022-6063.
10. Hicks, J. W.; Parkes, J.; Tong, J.; Houle, S.; Vasdev, N.; Wilson, A. A. Radiosynthesis and ex vivo evaluation of [(11)C-carbonyl]carbamate- and urea-based monoacylglycerol lipase inhibitors. *Nuclear Medicine Biology* **2014,** 41, 688-94.
11. Cherry, S. R. Fundamentals of positron emission tomography and applications in preclinical drug development. *The Jouranl of Clinical Pharmacology* **2001,** 41, 482-491.
12. Patel, S.; Gibson, R. In vivo site-directed radiotracers: a mini-review. *Nuclear Medicine and Biology* **2008,** 35, 805-815.
13. Phelps, M. E. Positron emission tomography provides molecular imaging of biological processes. *Proceedings of the National Academy of Sciences of the United States of America* **2000,** 97, 9226-9233.
14. Ogasawara, D.; Deng, H.; Viader, A.; Baggelaar, M. P.; Breman, A.; den Dulk, H.; van den Nieuwendijk, A. M.; Soethoudt, M.; van der Wel, T.; Zhou, J.; Overkleeft, H. S.; Sanchez-Alavez, M.; Mo, S.; Nguyen, W.; Conti, B.; Liu, X.; Chen, Y.; Liu, Q. S.; Cravatt, B. F.; van der Stelt, M. Rapid and profound rewiring of brain lipid signaling networks by acute diacylglycerol lipase inhibition. *Proceedings of the National Academy of Sciences of the United States of America* **2016,** 113, 26-33.
15. van den Nieuwendijk, A. M.; Ruben, M.; Engelsma, S. E.; Risseeuw, M. D.; van den Berg, R. J.; Boot, R. G.; Aerts, J. M.; Brussee, J.; van der Marel, G. A.; Overkleeft, H. S. Synthesis of L-altro-1-deoxynojirimycin, D-allo-1-deoxynojirimycin, and D-galacto-1-deoxynojirimycin from a single chiral cyanohydrin. *Organic letters* **2010,** 12, 3957-3959.
16. Zweemer, A. J. M.; Nederpelt, I.; Vrieling, H.; Hafith, S.; Doornbos, M. L. J.; de Vries, H.; Abt, J.; Gross, R.; Stamos, D.; Saunders, J.; Smit, M. J.; IJzerman, A. P.; Heitman, L. H.

Multiple binding sites for small-molecule antagonists at the CC chemokine receptor 2. *Molecular Pharmacology* **2013,** 84, 551-561.

17. Liu, Y.; Patricelli, M. P.; Cravatt, B. F. Activity-based protein profiling: the serine hydrolases. *Proceedings of the National Academy of Sciences of the United States of America* **1999,** 96, 14694-14699.

18. Kidd, D.; Liu, Y.; Cravatt, B. F. Profiling serine hydrolase activities in complex proteomes. *Biochemistry* **2001,** 40, 4005-4015.

19. Patricelli, M. P.; Giang, D. K.; Stamp, L. M.; Burbaum, J. J. Direct visualization of serine hydrolase activities in complex proteomes using fluorescent active site-directed probes. *Proteomics* **2001,** 1, 1067-1071.

20. Hsu, K.-L. L.; Tsuboi, K.; Adibekian, A.; Pugh, H.; Masuda, K.; Cravatt, B. F. DAGLβ inhibition perturbs a lipid network involved in macrophage inflammatory responses. *Nature Chemical Biology* **2012,** 8, 999-1007.

21. Baggelaar, M. P.; Janssen, F. J.; van Esbroeck, A. C.; den Dulk, H.; Allarà, M.; Hoogendoorn, S.; McGuire, R.; Florea, B. I.; Meeuwenoord, N.; van den Elst, H.; van der Marel, G. A.; Brouwer, J.; Di Marzo, V.; Overkleeft, H. S.; van der Stelt, M. Development of an activity-based probe and in silico design reveal highly selective inhibitors for diacylglycerol lipase-α in brain. *Angewandte Chemie International Edition* **2013,** 52, 12081-12085.

22. Zweemer, A. J.; Nederpelt, I.; Vrieling, H.; Hafith, S.; Doornbos, M. L.; de Vries, H.; Abt, J.; Gross, R.; Stamos, D.; Saunders, J.; Smit, M. J.; Ijzerman, A. P.; Heitman, L. H. Multiple binding sites for small-molecule antagonists at the CC chemokine receptor 2. *Molecular pharmacology* **2013,** 84, 551-561.